The Analysis of Valve-Controlled Hydraulic Servomechanisms

By R. G. RAUSCH

(Manuscript received July 10, 1959)

The nonlinear equations that represent the behavior of valve-controlled hydraulic servomechanisms are derived, and the assumptions necessary for their linearization are discussed. Solutions of the nonlinear equations obtained by analog computation are compared with solutions of the linear equations. Attention is directed to the influence of the hydraulic parameters on the nonlinear closed-loop system behavior.

I. INTRODUCTION

Since the development of hydraulic control valves such as that employed in the Nike missile,[1] emphasis has been given to the analysis of hydraulic phenomena in valved systems,[2,3,4] with much of the literature having been devoted to hydraulic component design. In this paper, the nonlinear closed-loop performance is given major emphasis; the effect of hydraulic parameter variations on the closed-loop frequency and transient responses is examined by linear and nonlinear methods.

The basic servomechanism under consideration in this study, as shown in Fig. 1, consists of a summing device, an amplifier, a flow source and control system, a hydraulic actuator (or motor) and a load. In the following sections, the nonlinear differential equations which represent the behavior of this closed-loop system are derived, a linear and an incremental-linear representation are discussed and solutions of the nonlinear equations obtained by analog computation are compared with linear solutions.

II. MOTOR AND LOAD ANALYSIS

In this section, emphasis is on the derivation and validity of the equations used to represent the behavior of the actuator and load; the mechanization of the flow source and its method of control will be discussed in detail in the following section.

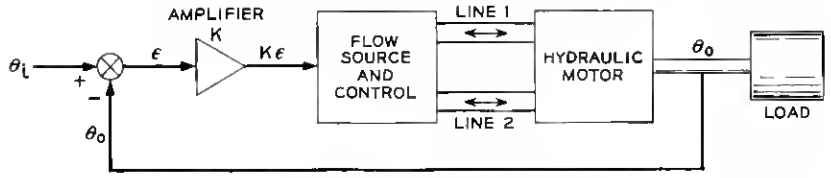

Fig. 1 — Basic hydraulic positional servomechanism.

In Fig. 2, a piston-type actuator is shown connected hydraulically to a flow source and mechanically to a load. The initial step in the analysis is to relate the flows Q_1 and Q_2 to the dependent variable x, the piston displacement from the center position.

The instantaneous volumes between the piston and two arbitrary sections in the lines leading to the cylinder are designated V_{T1} and V_{T2} (in cubic inches), the numerical subscripts indicating a particular side of the piston. Q_1 and Q_2 (in cubic inches per second) represent the flows from the source and depend upon the source mechanization; they are considered positive in the directions indicated in the diagram. Q_L, the leakage flow past the piston, is also shown in the assumed positive direction.

A control volume is chosen so that it coincides with the volume V_{T1} (where V_{T1} is a function of time) and the equation for the conservation of mass flow is written for this volume. This relationship states that the rate of mass accumulation in the control volume is equal to the net rate of mass flow into the volume. The net rate of mass flow into V_{T1} is given by

$$\text{net rate of mass flow into } V_{T1} = \rho(Q_1 - Q_L), \tag{1}$$

where ρ is the mass density (in pound-seconds^2 per inch^4) of the fluid and Q_L is the flow out of V_{T1}.

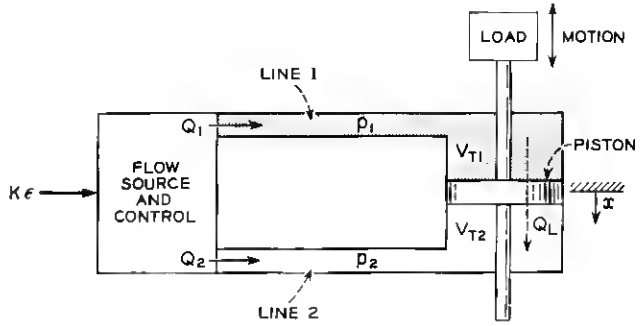

Fig. 2 — Variable displacement actuator.

In writing (1), it is assumed that the mass density, ρ, is uniform throughout the control volume; i.e., it is assumed that ρ is a function of time only, and not a function of position in the volume. Since ρ is dependent upon the instantaneous pressure, p_1, existing in V_{T1}, this assumes that p_1 is uniform throughout V_{T1}. The justification for this assumption is based on the calculation of the velocity of propagation of a longitudinal compression wave in the fluid. In general, the velocity of propagation, for adiabatic conditions, is given by

$$v_p = \sqrt{\frac{\beta}{\rho}}, \tag{2}$$

where β is the adiabatic bulk modulus of compression of the fluid. For a typical oil, v_p is approximately 50,000 inches per second. If the largest linear dimension of the volume V_{T1} is small, the pressure wave will complete many cycles in a short time, and the perturbation will be rapidly attenuated. For valve-controlled high-performance systems, the volumes are small; under the assumption that the largest dimension is one inch, the time of travel is 0.02 millisecond. Since this value is small compared to system time constants of the order of five milliseconds or more, the pressure can be assumed uniform throughout the volume. A calculation of the frequency of oscillation at which nonuniform pressure distribution becomes important shows that it is much higher than the frequencies of interest: 10,000 cps versus 200 cps.

The rate of mass accumulation in the volume V_{T1} is given by

$$\text{rate of mass accumulation in } V_{T1} = \frac{d(\rho V_{T1})}{dt} = \rho \dot{V}_{T1} + V_{T1}\dot{\rho}. \tag{3}$$

Equating (1) to (3) and solving for Q_1 yields

$$Q_1 = Q_L + \dot{V}_{T1} + \frac{V_{T1}}{\rho}\dot{\rho}. \tag{4}$$

The adiabatic bulk modulus of compression, β, of the fluid is defined as

$$\beta = \frac{dp}{\left(\frac{d\rho}{\rho}\right)}, \tag{5}$$

where β is assumed constant. The elimination of ρ from (4) by use of (5) results in

$$Q_1 = Q_L + \dot{V}_{T1} + \frac{V_{T1}}{\beta}\dot{p}_1. \tag{6}$$

In the same manner, application of the equation for the conservation of mass flow to the volume V_{T2} yields

$$Q_2 = -Q_L + \dot{V}_{T2} + \frac{V_{T2}}{\beta}\dot{p}_2. \tag{7}$$

Experimental tests show that the leakage flow is proportional to the pressure differential across the motor (laminar flow), so that

$$Q_L = L_m(p_1 - p_2), \tag{8}$$

where L_m is the leakage coefficient (in inches^5 per pound-second) of the actuator. In addition, define

$$V_T = \frac{V_{T1} + V_{T2}}{2}, \tag{9}$$

where V_T is a constant, so that

$$\begin{aligned} V_{T1} &= V_T + Ax, \\ V_{T2} &= V_T - Ax, \end{aligned} \tag{10}$$

where A is the cross-sectional area (in square inches) of the piston and x (in inches) is the piston displacement measured from the center position. Equations (6) and (7) are thus

$$Q_1 = L_m(p_1 - p_2) + A\dot{x} + \frac{(V_T + Ax)}{\beta}\dot{p}_1 \tag{11}$$

and

$$Q_2 = -L_m(p_1 - p_2) - A\dot{x} + \frac{(V_T - Ax)}{\beta}\dot{p}_2\,. \tag{12}$$

These flow equations have been developed for the linear piston-type actuator, but the same equations are valid for vane motors.

For a fixed-stroke axial-piston rotary motor, the control volume V_{T1} is a discontinuous function of time, since, as the cylinder block rotates, the individual cylinders transfer from one side of the motor to the other. Since the volume of one cylinder is small compared to the total volume on one side of the motor, the volume variation due to this discontinuity may be neglected without serious error. Thus, the control volume V_{T1} is essentially constant, so that

$$V_{T1} = V_{T2} = V_T\,, \tag{13}$$

where V_T is constant and is equal to one-half of the volume in the

system. With this assumption, the flow equations for the fixed-stroke axial-piston motor can be written

$$Q_1 = L_m(p_1 - p_2) + V_m\dot{\theta}_0 + \frac{V_T}{\beta}\dot{p}_1 \tag{14}$$

and

$$Q_2 = -L_m(p_1 - p_2) - V_m\dot{\theta}_0 + \frac{V_T}{\beta}\dot{p}_2, \tag{15}$$

where $\dot{\theta}_0$ is the motor shaft angular rate and V_m (in cubic inches per radian) is the fluid displacement per unit rotation of the motor shaft. Since V_T and β do not occur separately in (14) and (15), it will be convenient to define a "compliance coefficient" K_c as

$$K_c = \frac{V_T}{\beta}, \tag{16}$$

where K_c has the units of inches^5 per pound.

The remaining discussion will be concerned with a rotational system, for which (14) and (15) have been developed; the same relationships will be valid for a translational system having small displacement x, with appropriate changes in the definitions of the parameters.

In addition to the flow equations, two torque equations can be derived. The first is an energy relationship that equates the work done by the forces on the motor during a rotational of θ_0 radians to the work output from the motor shaft. The work input is $(p_1 - p_2)\ V_m\theta_0$ and is the flow work commonly encountered in the Bernoulli equation. The corresponding work output is $T\theta_0$, where T is the opposing torque. Since these two expressions for work must be equal, there results

$$T = (p_1 - p_2)\ V_m. \tag{17}$$

Another torque equation is obtained from Newton's Second Law of Motion. In general, the load may consist of inertia, damping and friction torques, and disturbing torques. Thus, the following equation may be written:

$$T = J\ddot{\theta}_0 + T_0, \tag{18}$$

where J (in pound-inch-seconds^2) is the total inertia (including that of the motor and fluid) referred to the motor shaft, and T_0 (in pound-inches) is the total friction and disturbing torque acting on the motor shaft.

The elimination of T from (17) and (18) results in

$$(p_1 - p_2)\, V_m = J\ddot{\theta}_0 + T_0\,. \tag{19}$$

A restriction must be placed on the values allowable for the pressures p_1 and p_2. If absolute pressure units are employed, these pressures must always be equal to or greater than zero. A more accurate representation would be obtained if the vaporization pressure were considered as the limiting value, but, in view of the fact that the differential pressures in the system are normally very large, this degree of refinement is not warranted. A good approximation is

$$p_1 \geqq 0 \qquad \text{and} \qquad p_2 \geqq 0, \tag{20}$$

where it is understood that absolute pressure units are employed.

In addition to the equations derived, the usual expression for the position error ϵ in terms of the input angle θ_i and the output angle θ_0 for a servomechanism having unity feedback (as in Fig. 1) is given by

$$\epsilon = \theta_i - \theta_0\,. \tag{21}$$

The equations which have been derived in this section and which apply to the axial-piston rotary motor are summarized below:

$$\begin{aligned} Q_1 &= L_m(p_1 - p_2) + V_m\dot{\theta}_0 + K_c\dot{p}_1\,, \\ Q_2 &= -L_m(p_1 - p_2) - V_m\dot{\theta}_0 + K_c\dot{p}_2\,, \\ (p_1 - p_2)\, V_m &= J\ddot{\theta}_0 + T_0\,, \\ p_1 &\geqq 0 \qquad \text{and} \qquad p_2 \geqq 0, \\ \epsilon &= \theta_i - \theta_0\,. \end{aligned} \tag{22}$$

The units employed in these equations are given in Table I.

The expressions for Q_1 and Q_2, the flows from the controlled source, are discussed in the next section.

III. CONTROL-VALVE ANALYSIS

In Section II, the equations relating the flows (into the motor) to the dynamic state of the system were derived; the expressions for the flows Q_1 and Q_2 were not specified. In this section, these quantities are discussed for the particular case of a valve-controlled system and analytical expressions relating flow to error signal and pressure are obtained.

The schematic diagram of a typical valve configuration is given in

TABLE I — DEFINITIONS OF SYMBOLS; UNITS

Symbol	Definition	Units
Q	flow	in^3/sec
L_m	motor leakage coefficient	$in^5/lb\text{-}sec$
p	pressure	lb/in^2
V_m	motor displacement	$in^3/radian$
θ_i	position angle input	radians
θ_0	position angle output	radians
ϵ	position angular error	radians
V_T	one-half total trapped volume	in^3
β	bulk modulus of compression	lb/in^2
J	total inertia	$lb\text{-}in\text{-}sec^2$
K_c	compliance coefficient	in^5/lb
T_0	viscous, friction and disturbing torque	lb-in
ρ	fluid mass density	$lb\text{-}sec^2/in^4$

Fig. 3. The type of actuator is not important in this discussion and, for simplicity, it is pictured as a translational piston.

A source having a pressure p_s supplies fluid to the valve as shown and the main spool controls the direction and magnitude of this flow to the motor. Fluid is returned to a sump at pressure p_d. As in Section II, the pressure on each side of the actuator piston is designated as p with the appropriate numerical subscript.

The main spool controls the flow by means of four orifices O_1, O_2, E_1 and E_2, and the spool position, in turn, is controlled by a transducer. The configuration of the transducer varies considerably in current

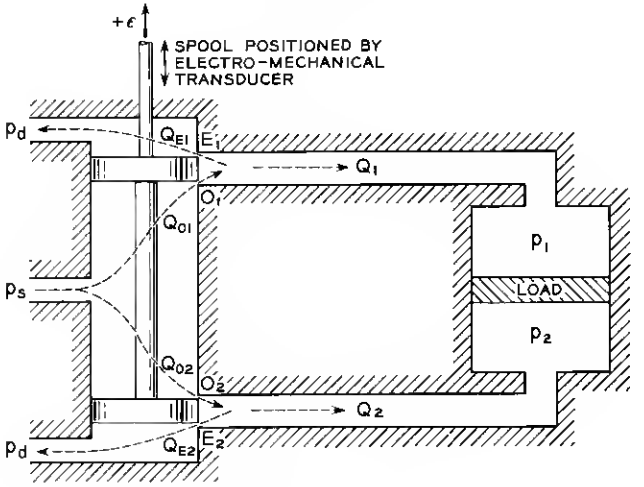

Fig. 3 — Orifice flow conventions.

production models and may have the form of either a torque motor or a hydraulic preamplifier preceded by a torque motor or solenoid. If a hydraulic preamplifier is employed, the entire valve is designated as a "two-stage" valve. In the analysis an ideal spool-positioning mechanism will be assumed; i.e., there will be only one position of the valve spool corresponding to a given error signal, ϵ.

The following nodal equations are obtained from Fig. 3:

$$\begin{aligned} Q_1 &= Q_{O1} - Q_{E1}\,, \\ Q_2 &= Q_{O2} - Q_{E2}\,. \end{aligned} \tag{23}$$

Here, as in Section II, the flows are chosen positive in the directions indicated in the figure.

It is necessary to express the flows through the orifices in terms of the pressures and the orifice openings. Consider first the general orifice equation; application of Bernoulli's equation to the case of flow through an orifice of area A results in the relation

$$Q = \frac{AC_cC_v}{\sqrt{1 - C_c^2\left(\frac{A}{A_1}\right)^2}} \sqrt{\frac{2\Delta p}{\rho}}\,, \tag{24}$$

where:

Q = flow,
A = orifice area,
C_c = orifice contraction coefficient,
C_v = velocity coefficient,
A_1 = upstream line area,
Δp = pressure differential across the orifice,
ρ = mass density of the fluid.

For application to a valve orifice, note that A/A_1 is small compared to unity and that C_c is less than unity. It follows, therefore, that a good approximation is obtained by

$$Q = AC_cC_v \sqrt{\frac{2\Delta p}{\rho}}\,. \tag{25}$$

The usual procedure in hydraulics is to define a discharge coefficient, C, as

$$C = C_cC_v\,, \tag{26}$$

so that (25) becomes

$$Q = AC \sqrt{\frac{2\Delta p}{\rho}}\,. \tag{27}$$

This equation has been derived for the steady-state flow through an orifice; in the analysis, it will be assumed that the same relationship is valid for the dynamic state. It is not necessary to assume a value for the discharge coefficient C, since it will be included in an over-all gain constant.

In the present application, the orifice area, A, is proportional to the displacement of the valve spool (assuming rectangular orifices) and the displacement is proportional to the electrical activating signal, $K\epsilon$, received by the positioning mechanism (see Fig. 3). It follows that A is proportional to $K\epsilon$, and (27) may be written as

$$Q = (K\epsilon)C_0 \sqrt{\frac{\Delta p}{\rho}}, \tag{28}$$

where C_0 is a new coefficient that is proportional to the area of the orifice per radian of input signal. If the mass density, ρ, of the fluid is assumed constant in this expression, the following equation may be written:

$$Q = (K_b\epsilon) \sqrt{\Delta p}, \tag{29}$$

where

$$K_b = \frac{KC_0}{\rho^{1/2}} \tag{30}$$

is a constant for a given system. K_b has the units of inches^4 per pound$^{1/2}$-second-radians.

The relationship of (29) is indicated graphically in Fig. 4. In this figure, the equation has been normalized with respect to the three maximum values $Q_{\max}$, $(K_b\epsilon)_{\max}$ and $\Delta p_{\max}$. Since there is a limit to the magnitude of the spool displacement, a spool-displacement saturation region is indicated. (Spool-displacement saturation occurs when the electrical error signal becomes greater than that corresponding to the maximum valve spool-displacement; i.e., the error signal demands a spool position that is physically impossible.)

Equation (29) implies that the flow through the orifice is zero for zero error ϵ. This is not generally true for the orifices in most valves, and in fact, this condition would be very difficult to obtain. Equation (29) must be specialized for each orifice.

There are three general types of valves, which can be classified according to the flow conditions at zero signal input ϵ; these are: (a) the open-center valve, (b) the critical-center valve and (c) the closed-center

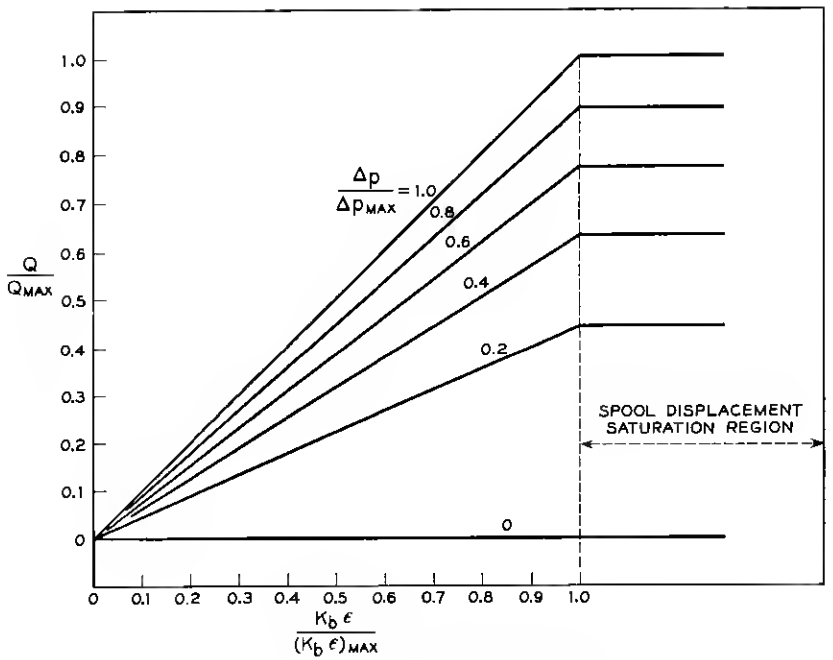

Fig. 4 — Orifice flow characteristics.

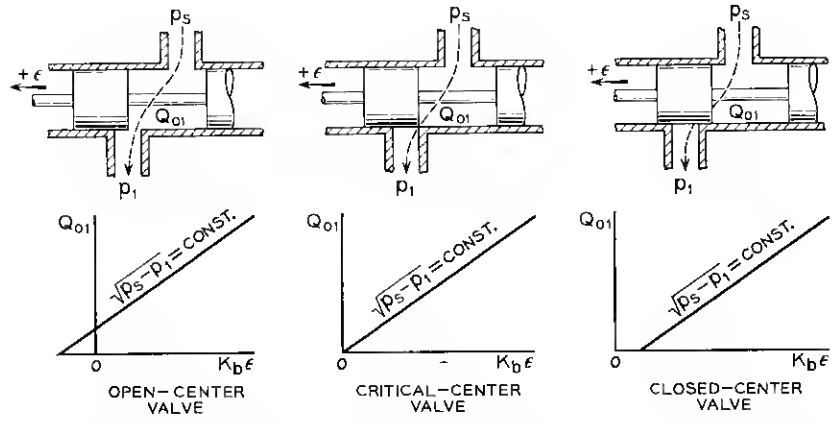

Fig. 5 — (a) Neutral position for the three basic valve types; (b) typical characteristics for the three basic valve types.

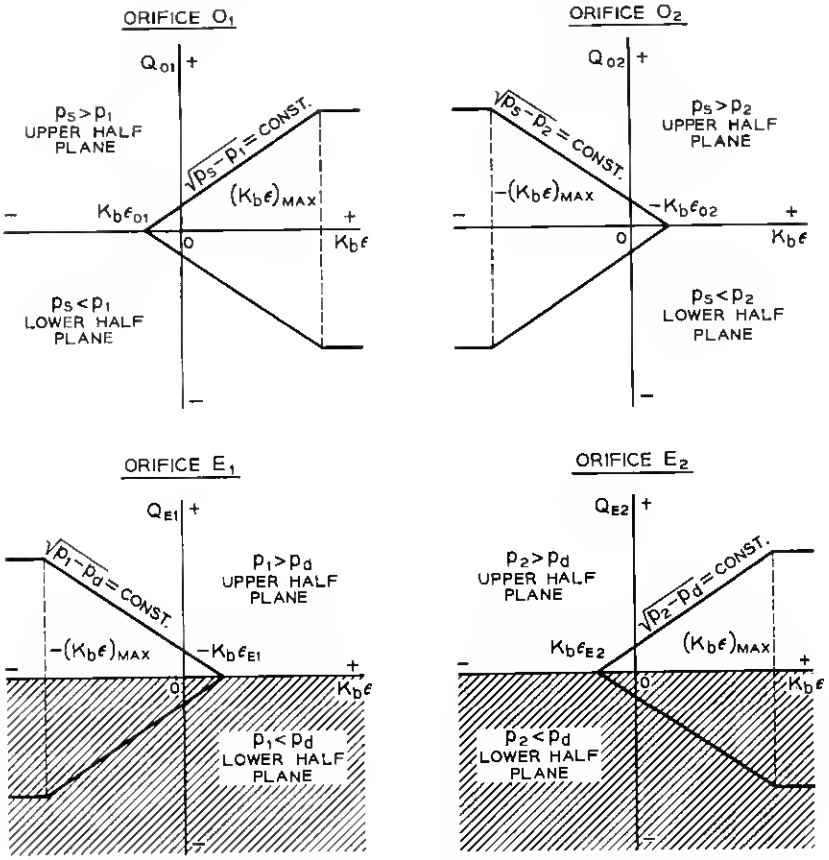

Fig. 6 — Flow characteristics for the orifices in an open-center valve.

valve. Fig. 5(a) indicates the zero error position of the spool for each of these types for the orifice O_1. In the open-center valve, flow passes through the orifice for the condition $\epsilon = 0$, i.e., for the spool in the neutral position. The critical-center valve allows no flow to pass in the neutral position; however, a slight positive displacement opens the orifice O_1. The closed-center valve has a dead zone in that a relatively large displacement is required to open the orifice from the neutral position.

Fig. 5(b) shows a typical differential isobar (corresponding to those of Fig. 4) for each type of valve. The origin is translated according to the neutral spool position.

It is now possible to express the individual orifice flows as shown in Fig. 3 with the aid of Fig. 6 and (29). Fig. 6 shows a typical differential

isobar for each of the four orifices O_1, O_2, E_1 and E_2, the case shown representing the open-center type valve. (The equations to be derived will be applicable to all three valve types, depending upon the choice of the neutral position error-flow constants.) It should be noted that the direction of flow is dependent on the sign of Δp for each orifice. In general, the equations for the flows are as given by (31). In these equations ϵ_{O1}, ϵ_{O2}, ϵ_{E1}, ϵ_{E2} are positive for an open-center valve, $\epsilon_{\max}$ is taken as positive and sgn denotes the signum (sign) function:

$$
\begin{aligned}
Q_{O1} &= \begin{cases} K_b\,|\,\epsilon_{\max} + \epsilon_{O1}\,|\,\sqrt{|\,p_s - p_1\,|}\ \operatorname{sgn}\,(p_s - p_1) & \epsilon > \epsilon_{\max} \\ K_b\,|\,\epsilon + \epsilon_{O1}\,|\,\sqrt{|\,p_s - p_1\,|}\ \operatorname{sgn}\,(p_s - p_1) & -\epsilon_{O1} < \epsilon < \epsilon_{\max} \\ 0 & \epsilon < -\epsilon_{O1}, \end{cases} \\
Q_{O2} &= \begin{cases} 0 & \epsilon > \epsilon_{O2} \\ K_b\,|\,\epsilon - \epsilon_{O2}\,|\,\sqrt{|\,p_s - p_2\,|}\ \operatorname{sgn}\,(p_s - p_2) & -\epsilon_{\max} < \epsilon < \epsilon_{O2} \\ K_b\,|\,\epsilon_{\max} - \epsilon_{O2}\,|\,\sqrt{|\,p_s - p_2\,|}\ \operatorname{sgn}\,(p_s - p_2) & \epsilon < -\epsilon_{\max}, \end{cases} \\
Q_{E1} &= \begin{cases} 0 & \epsilon > \epsilon_{E1} \\ K_b\,|\,\epsilon - \epsilon_{E1}\,|\,\sqrt{|\,p_1 - p_d\,|}\ \operatorname{sgn}\,(p_1 - p_d) & -\epsilon_{\max} < \epsilon < \epsilon_{E1} \\ K_b\,|\,\epsilon_{\max} - \epsilon_{E1}\,|\,\sqrt{|\,p_1 - p_d\,|}\ \operatorname{sgn}\,(p_1 - p_d) & \epsilon < -\epsilon_{\max}, \end{cases} \\
Q_{E2} &= \begin{cases} K_b\,|\,\epsilon_{\max} + \epsilon_{E2}\,|\,\sqrt{|\,p_2 - p_d\,|}\ \operatorname{sgn}\,(p_2 - p_d) & \epsilon > \epsilon_{\max} \\ K_b\,|\,\epsilon + \epsilon_{E2}\,|\,\sqrt{|\,p_2 - p_d\,|}\ \operatorname{sgn}\,(p_2 - p_d) & -\epsilon_{E2} < \epsilon < \epsilon_{\max} \\ 0 & \epsilon < -\epsilon_{E2}; \end{cases}
\end{aligned}
\tag{31}
$$

Simplification of (31) is obtained by assuming that the sump pressure

TABLE II — DEFINITIONS OF SYMBOLS; UNITS

Symbol	Definition	Units
Q	flow	in^3/sec
A	orifice area	in^2
A_1	upstream line area	in^2
C_c	orifice contraction coefficient	—
C_v	orifice velocity coefficient	—
C	orifice discharge coefficient	—
C_0	area per radian input	in^2/rad
ϵ	angular actuating signal	radians
K	dimensionless gain constant	—
K_b	over-all gain constant	$in^4/lb^{1/2}$-sec-rad
p	pressure	lb/in^2
Δp	differential pressure	lb/in^2
ρ	fluid mass density	$lb\text{-}sec^2/in^4$

p_d is zero psi absolute rather than atmospheric pressure; this is a good approximation since the pressure differentials are usually several hundred psi. This assumption eliminates consideration of the shaded regions in Fig. 6 for the orifices E_1 and E_2. Furtber simplification is obtained if the valve is assumed to be perfectly symmetrical; i.e.,

$$\epsilon_{O1} = \epsilon_{O2} = \epsilon_{E1} = \epsilon_{E2} = \epsilon_0 ,$$

and if it is assumed that the maximum spool position is never attained. With these assumptions, (31) simplify to (32):

$$\begin{aligned}
Q_{O1} &= \begin{cases} K_b |\epsilon + \epsilon_0| \sqrt{|p_s - p_1|}\ \operatorname{sgn}(p_s - p_1) & \epsilon > -\epsilon_0 \\ 0 & \epsilon < -\epsilon_0 , \end{cases} \\
Q_{O2} &= \begin{cases} 0 & \epsilon > \epsilon_0 \\ K_b |\epsilon - \epsilon_0| \sqrt{|p_s - p_2|}\ \operatorname{sgn}(p_s - p_2) & \epsilon < \epsilon_0 , \end{cases} \\
Q_{E1} &= \begin{cases} 0 & \epsilon > \epsilon_0 \\ K_b |\epsilon - \epsilon_0| \sqrt{p_1} & \epsilon < \epsilon_0 , \end{cases} \\
Q_{E2} &= \begin{cases} K_b |\epsilon + \epsilon_0| \sqrt{p_2} & \epsilon > -\epsilon_0 \\ 0 & \epsilon < -\epsilon_0 . \end{cases}
\end{aligned} \tag{32}$$

These equations, together with (23) and (22), complete the preliminary analysis for the valve-controlled servomechanism. Definitions of the symbols, together with a consistent set of units, are given in Table II.

IV. LINEAR AND INCREMENTAL-LINEAR ANALYSIS

The linearization of the equations representing the motor as given by (22) results in (for a pure inertial load):

$$\begin{aligned}
Q_1 &= L_m(p_1 - p_2) + V_m\dot{\theta}_0 + K_c\dot{p}_1 , \\
Q_2 &= -L_m(p_1 - p_2) - V_m\dot{\theta}_0 + K_c\dot{p}_2 , \\
(p_1 - p_2)\, V_m &= J\ddot{\theta}_0 , \\
\epsilon &= \theta_i - \theta_0 .
\end{aligned} \tag{33}$$

The restrictions on the values of p_1 and p_2 and their derivatives are not applicable to a linear theory and have been omitted; in addition, the friction and output disturbing torques have been assumed to be zero.

For the case of a symmetrical valve having characteristics as given by (32), the flows through the orifices are functions of the gain constant, K_b, the error signal, ϵ, the open-center constant, ϵ_0, and the respective

orifice pressure drops. If the region of applicability is restricted to those cases in which $p_s > p_1$ and $p_s > p_2$ (pressures not limited) and in which $| \epsilon | < | \epsilon_{max} |$, (32) may be written:

$$\begin{aligned} Q_{O1} &= K_b(\epsilon + \epsilon_0)\sqrt{p_s - p_1} && \text{for} \quad \epsilon > -\epsilon_0 , \\ Q_{O2} &= -K_b(\epsilon - \epsilon_0)\sqrt{p_s - p_2} && \text{for} \quad \epsilon < \epsilon_0 , \\ Q_{E1} &= -K_b(\epsilon - \epsilon_0)\sqrt{p_1} && \text{for} \quad \epsilon < \epsilon_0 , \\ Q_{E2} &= K_b(\epsilon + \epsilon_0)\sqrt{p_2} && \text{for} \quad \epsilon > -\epsilon_0 . \end{aligned} \tag{34}$$

From (23) and (34) it can be seen that there are three distinct ranges of ϵ that must be considered, the magnitude of the range depending upon the value of ϵ_0 :

Region A ($| \epsilon | \leqq \epsilon_0$):

$$\begin{aligned} Q_1 &= K_b(\epsilon + \epsilon_0)\sqrt{p_s - p_1} + K_b(\epsilon - \epsilon_0)\sqrt{p_1} , \\ Q_2 &= -K_b(\epsilon - \epsilon_0)\sqrt{p_s - p_2} - K_b(\epsilon + \epsilon_0)\sqrt{p_2} . \end{aligned} \tag{35}$$

Region B+ ($\epsilon \geqq \epsilon_0$):

$$\begin{aligned} Q_1 &= K_b(\epsilon + \epsilon_0)\sqrt{p_s - p_1} , \\ Q_2 &= -K_b(\epsilon + \epsilon_0)\sqrt{p_2} . \end{aligned} \tag{36}$$

Region B− ($\epsilon \leqq \epsilon_0$):

$$\begin{aligned} Q_1 &= K_b(\epsilon - \epsilon_0)\sqrt{p_1} , \\ Q_2 &= -K_b(\epsilon - \epsilon_0)\sqrt{p_s - p_2} . \end{aligned} \tag{37}$$

Expanding $\sqrt{p_s - p}$ and $\sqrt{p}$ about the steady-state value $p_s/2$ yields

Region A:

$$Q_1 - Q_2 = 2K_b \left(2\epsilon \sqrt{\frac{p_s}{2}} - \epsilon_0 \frac{p_1 - p_2}{\sqrt{2p_s}} \right). \tag{38}$$

Region B+:

$$Q_1 - Q_2 = K_b (\epsilon + \epsilon_0) \left(2\sqrt{\frac{p_s}{2}} - \frac{p_1 - p_2}{\sqrt{2p_s}} \right). \tag{39}$$

Region B−:

$$Q_1 - Q_2 = K_b(\epsilon - \epsilon_0) \left(2\sqrt{\frac{p_s}{2}} + \frac{p_1 - p_2}{\sqrt{2p_s}} \right), \tag{40}$$

where the higher-order terms in $[(p_s/2) - p]$ have been neglected. This

further restricts the region of validity of our analysis to those cases where the pressure differential across the load is not large.

For the region A, combination of (33) and (38) results in

$$4K_b\sqrt{\frac{p_s}{2}}\,\epsilon = \frac{K_cJ}{V_m}\dddot{\theta}_0 + \frac{2J}{V_m}\left(L_m + \frac{K_b\epsilon_0}{\sqrt{2p_s}}\right)\ddot{\theta}_0 + 2V_m\dot{\theta}_0, \tag{41}$$

and the open-loop transfer function becomes

$$G_A(s) = \frac{\theta_0(s)}{\epsilon(s)} = \frac{\dfrac{4V_mK_b}{K_cI}\sqrt{\dfrac{p_s}{2}}}{s\left[s^2 + \dfrac{2}{K_c}\left(L_m + \dfrac{K_b\epsilon_0}{\sqrt{2p_s}}\right)s + \dfrac{2V_m^2}{K_cJ}\right]}, \tag{42}$$

or

$$G_A(s) = \frac{\theta_0(s)}{\epsilon(s)} = \frac{\dfrac{\omega_a}{\omega_n}}{\left(\dfrac{s}{\omega_n}\right)\left[\left(\dfrac{s}{\omega_n}\right)^2 + 2\zeta_a\left(\dfrac{s}{\omega_n}\right) + 1\right]}, \tag{43}$$

where

$$\omega_n = V_m\sqrt{\frac{2\beta}{V_TJ}}, \tag{44}$$

$$\zeta_a = \frac{1}{V_m}\left[L_m + \frac{K_b\epsilon_0}{\sqrt{2p_s}}\right]\sqrt{\frac{J\beta}{2V_T}}, \tag{45}$$

$$\omega_a = \frac{2K_b}{V_m}\sqrt{\frac{p_s}{2}}. \tag{46}$$

Here, ω_n is the undamped natural frequency of the system, ζ_a is the damping ratio and ω_a is the velocity gain constant. (The subscript "a" indicates the region A.) It is interesting to note that ζ_a, the damping ratio, is the sum of the motor damping (motor leakage) and a term related to the steady-state flow through the valve. The term, $K_b\epsilon_0/\sqrt{2p_s}$, contributes the major damping to the system. In the quiescent state, since $\epsilon = 0$ and $p_1 = p_2 = p_s/2$, it follows from (34) that

$$(Q_{O1})_s = (Q_{O2})_s = (Q_{E1})_s = (Q_{E2})_s = K_b\epsilon_0\sqrt{\frac{p_s}{2}}, \tag{47}$$

where the subscript "s" indicates quiescent values. Now designate

$$Q_s = (Q_{O1})_s + (Q_{O2})_s, \tag{48}$$

where Q_s is the quiescent (i.e. $\epsilon = 0$ and $\dot{\theta} = 0$) total flow from the

source, so that

$$Q_s = 2K_b\epsilon_0\sqrt{\frac{p_s}{2}}. \tag{49}$$

An effective leakage coefficient is given by

$$L_a = \left(L_m + \frac{K_b\epsilon_0}{\sqrt{2p_s}}\right) = \left(L_m + \frac{Q_s}{2p_s}\right) \tag{50}$$

and therefore (45) becomes

$$\zeta_a = \frac{L_a}{V_m}\sqrt{\frac{J\beta}{2V_T}}. \tag{51}$$

Now consider the region B+, where $\epsilon \geqq \epsilon_0$. The combination of (33) and (39) results in

$$2K_b\sqrt{\frac{p_s}{2}}(\epsilon + \epsilon_0) = \frac{K_cJ}{V_m}\ddot{\theta}_0 + \frac{2J}{V_m}\left[L_m + \frac{K_b(\epsilon + \epsilon_0)}{2\sqrt{2p_s}}\right]\ddot{\theta}_0 + 2V_m\dot{\theta}_0. \tag{52}$$

An approximate "incremental linear" transfer function may be obtained for this region by making the substitutions

$$\begin{aligned} \epsilon &= \epsilon^* + \Delta\epsilon, \\ \theta_0 &= \theta_0{}^* + \Delta\theta_0, \end{aligned} \tag{53}$$

where both the starred and the incremental symbols are considered as functions of time. The incremental variables are assumed small, so that their products may be neglected. In this manner, a linear equation in the incremental quantities can be obtained if the equation defining the starred variables [(52) with the symbols starred] is subtracted from that obtained by the substitutions indicated previously. Then, if the resultant equation, which is linear in the incremental variables, contains any starred quantities, these can be considered to be varying slowly with time — that is, essentially constant when compared with the incremental variations with time. Therefore, a quasilinear incremental transfer function can be obtained. In the present case, the incremental transfer function valid for a small constant-acceleration, α_0, will be derived. This will be used to obtain the incremental transfer function for constant-velocity operation.

Thus, the analysis is initiated by obtaining the linear equation in the incremental quantities as previously outlined; this equation is

$$\begin{aligned} 2K_b\left(\sqrt{\frac{p_s}{2}} - \frac{J\ddot{\theta}_0{}^*}{2V_m\sqrt{2p_s}}\right)\Delta\epsilon = \\ \frac{K_cJ}{V_m}\Delta\ddot{\theta}_0 + \frac{2J}{V_m}\left[L_m + \frac{K_b(\epsilon^* + \epsilon_0)}{2\sqrt{2p_s}}\right]\Delta\ddot{\theta}_0 + 2V_m\Delta\dot{\theta}_0. \end{aligned} \tag{54}$$

Noting that a similar equation may be obtained for the region B−, and denoting both regions by B, the following transfer function is obtained for operation about a constant acceleration α_0 :

$$G_B(s) = \frac{\Delta\theta_0(s)}{\Delta\epsilon(s)} = \frac{\dfrac{\omega_b}{\omega_n}}{\left(\dfrac{s}{\omega_n}\right)\left[\left(\dfrac{s}{\omega_n}\right)^2 + 2\zeta_b\left(\dfrac{s}{\omega_n}\right) + 1\right]}, \tag{55}$$

where

$$\omega_n = V_m\sqrt{\frac{2\beta}{V_T J}}, \tag{56}$$

$$\zeta_b = \frac{1}{V_m}\left[L_m + \frac{K_b(|\epsilon^*| + \epsilon_0)}{2\sqrt{2p_s}}\right]\sqrt{\frac{J\beta}{2V_T}}, \tag{57}$$

$$\omega_b = \frac{K_b}{V_m}\sqrt{\frac{p_s}{2}}\left(1 - \frac{J|\alpha_0|}{2V_m p_s}\right). \tag{58}$$

For an inertia load (no viscous or coulomb friction), (58) can be written:

$$\omega_b = \frac{K_b}{V_m}\sqrt{\frac{p_s}{2}}\left(1 - \frac{|\Delta p^*|}{2p_s}\right), \tag{59}$$

where Δp^* is the constant-differential pressure acting on the motor.

The preceding equations give an approximate solution for the case in which the acceleration α_0 is small; i.e., ϵ^* varies slowly with time. For this case, the incremental damping ratio ζ_b is appreciably increased over that given by (45) for the region A. The incremental gain constant ω_b is less than the gain constant in the A region as defined in (46); for Δp^* equal to p_s, the gain is down 12 db from that of the A region.

For operation about a constant velocity ω_i, ω_n and ζ_b remain as in (56) and (57), but the gain constant becomes

$$\omega_b = \frac{K_b}{V_m}\sqrt{\frac{p_s}{2}}. \tag{60}$$

In this case, the gain is down 6 db from that given for the A region. For constant-speed operation, $\theta_0^* = \omega_i t$, the error is given by

$$\epsilon^* = \sqrt{\frac{2}{p_s}}\left(\frac{V_m\omega_i}{K_b}\right) - \epsilon_0, \tag{61}$$

so that the effective leakage coefficient becomes:

$$L_b = L_m + \frac{K_b(|\epsilon^*| + \epsilon_0)}{2\sqrt{2p_s}} = L_m + \frac{V_m\omega_i}{2p_s}. \tag{62}$$

Thus, since the "displacement" motor flow is given by

$$Q_m = V_m\dot{\theta}_0 = V_m\omega_i\,, \tag{63}$$

the effective leakage coefficient is

$$L_b = L_m + \frac{Q_m}{2p_s}. \tag{64}$$

In many cases, L_m is small compared to Q_m so that the incremental damping is primarily a function of the motor speed.

The velocity-lag error, ϵ_v (steady-state position error under the conditions $\dot{\theta}_0 = \omega_i$ where ω_i is a constant rate input), is as follows for the two regions:

Region A:

$$\epsilon_v = \frac{\omega_i}{\omega_a} = \frac{V_m\omega_i}{K_b\sqrt{2p_s}}. \tag{65}$$

Region B:

$$|\,\epsilon_v\,| = \frac{2V_m\,|\,\omega_i\,|}{K_b\sqrt{2p_s}} - \epsilon_0\,, \tag{66}$$

where it is understood that $|\,\epsilon_v\,|$ is greater than ϵ_0. The velocity lag error for the B region is thus approximately twice that predicted by (65) if ϵ_0 is small compared to the lag error.

Some qualitative information on the nature of the system performance can be obtained by comparison of (43) and (55). In the region A (i.e., $|\,\epsilon\,| < \epsilon_0$), the system is essentially linear for small pressure differentials. In the region B ($|\,\epsilon\,| > \epsilon_0$), the system is nonlinear *even though* the pressure differentials are assumed small. In this region, the behavior is "amplitude sensitive"; as the error amplitude increases, the incremental gain decreases. The incremental damping increases with increasing error in the B region and is considerably greater than the damping in the A region; the incremental damping is proportional to the total flow through the valve. The velocity-lag error is, of course, greater in the B region.

The transfer function $G_A(s)$ as given by (43) was derived for a fully symmetrical valve; the analysis of an unsymmetrical valve shows that the basic form of the transfer function is similar to that for the symmetrical valve. For the unsymmetrical valve, however, the damping ratio and gain expressions differ from those of (45) and (46). The damping ratio is

$$\zeta_a = \frac{1}{V_m}\left[L_m + \frac{Q_s p_s}{8p_q(p_s - p_q)}\right]\sqrt{\frac{J\beta}{2V_T}}, \tag{67}$$

where p_q is the quiescent value of the pressures p_1 and p_2. For $p_q = p_s/2$, this expression is identical to that given by (45); for p_q greater or less than $p_s/2$, the damping is greater than that given by (45) (assuming the same quiescent flow Q_s). The gain constant is:

$$\omega_a = \frac{K_b}{V_m}(\sqrt{p_q} + \sqrt{p_s - p_q}), \tag{68}$$

and comparison with (46) shows that the two give the same solution for $p_q = p_s/2$. For p_q greater or less than $p_s/2$, the gain of the unsymmetrical valve is less than that of the symmetrical valve.

V. SOLUTIONS OF THE LINEARIZED EQUATIONS

The equations representing the valve-controlled servomechanism were linearized in the last section, and it was found that the open-loop transfer function had the following general form:

$$G(s) = \frac{\theta_0(s)}{\epsilon(s)} = \frac{\dfrac{\omega_0}{\omega_n}}{\left(\dfrac{s}{\omega_n}\right)\left[\left(\dfrac{s}{\omega_n}\right)^2 + 2\zeta\left(\dfrac{s}{\omega_n}\right) + 1\right]}, \tag{69}$$

where ω_0 is the velocity gain constant, ω_n the natural resonant frequency and ζ the dimensionless damping ratio. If this is considered as a frequency function, the resulting open-loop attenuation and phase vary as shown in Figs. 7 and 8. In these figures, the damping ratio, ζ, has been taken as a parameter.

Equation (69), when solved for the closed-loop function, results in

$$\frac{\theta_0(s)}{\theta_i(s)} = \frac{\dfrac{\omega_0}{\omega_n}}{\left(\dfrac{s}{\omega_n}\right)^3 + 2\zeta\left(\dfrac{s}{\omega_n}\right)^2 + \left(\dfrac{s}{\omega_n}\right) + \left(\dfrac{\omega_0}{\omega_n}\right)}. \tag{70}$$

The relationships for the closed-loop operation are exhibited graphically in Figs. 9 through 12. In Fig. 9, the gain margin is shown as a function of the peak attenuation, M_p (the maximum value of $|\theta_0/\theta_i|$), for the range of values of interest. In general, the gain margin decreases with increasing peak magnitude and is less for the lightly damped cases.

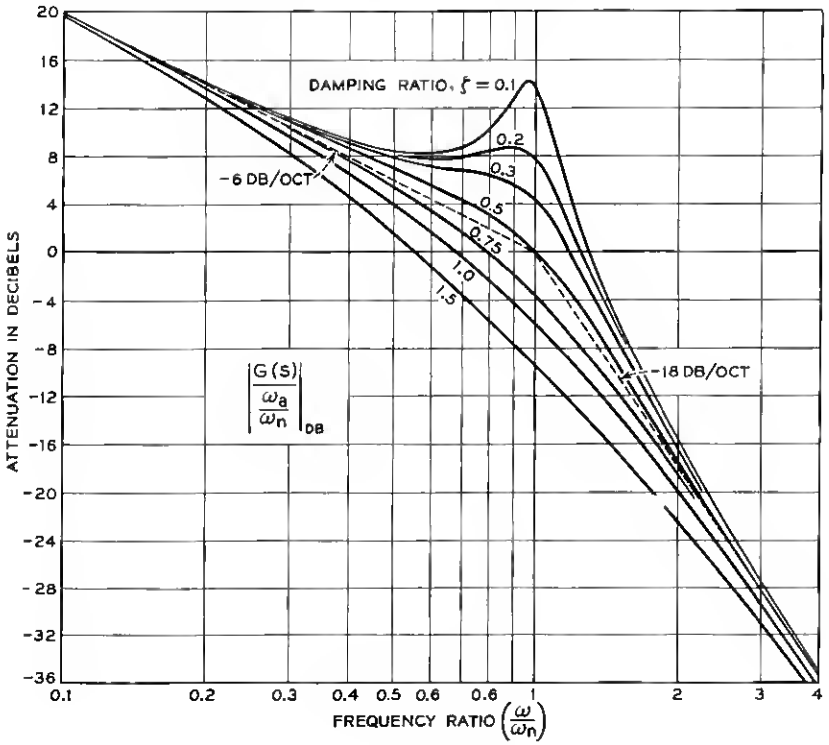

Fig. 7 — Open-loop attenuation of $G(s)$.

The phase margin variation with the peak magnitude is shown in Fig. 10; the smaller values of ζ have the largest phase margins.

Fig. 11 shows the variation of the peak frequency, ω_p, with the peak attenuation, M_p, for the various damping ratios ζ. For $\zeta = 0.1$, the peak frequency is approximately the undamped frequency of the system and is independent of the peak attenuation. As the damping is increased, the peak frequency decreases, and it is lower for the lower peak attenuations. In general, the lower the value of ω_p, the lower will be the bandwidth of the closed-loop system.

The relation between the velocity gain constant ω_0 and the peak magnitude is shown in Fig. 12 as a function of the damping ratio, ζ. As the gain constant is increased, the peak magnitude increases; in most cases (for constant peak magnitude), ω_0 is less for the lightly damped systems. This graph shows that, for $\zeta = 0.1$, a change in ω_0 of approximately 3 db is sufficient to cause M_p to increase 8 db, while,

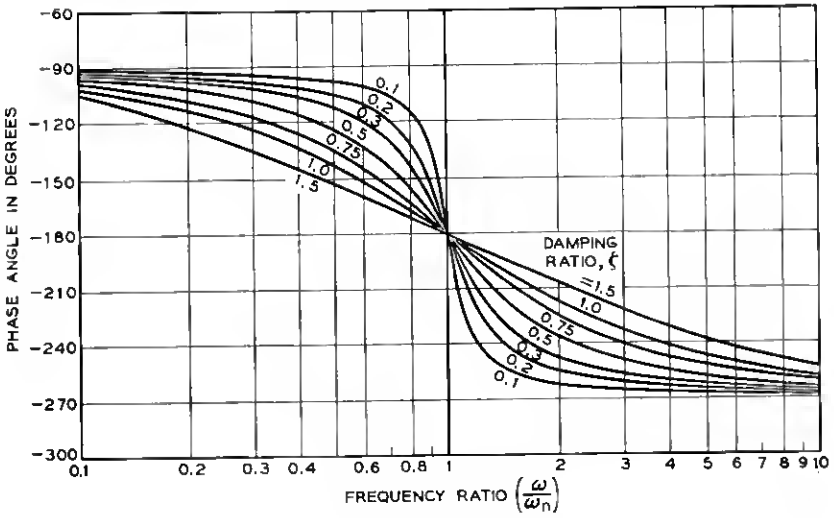

Fig. 8 — Open-loop phase angle of $G(s)$.

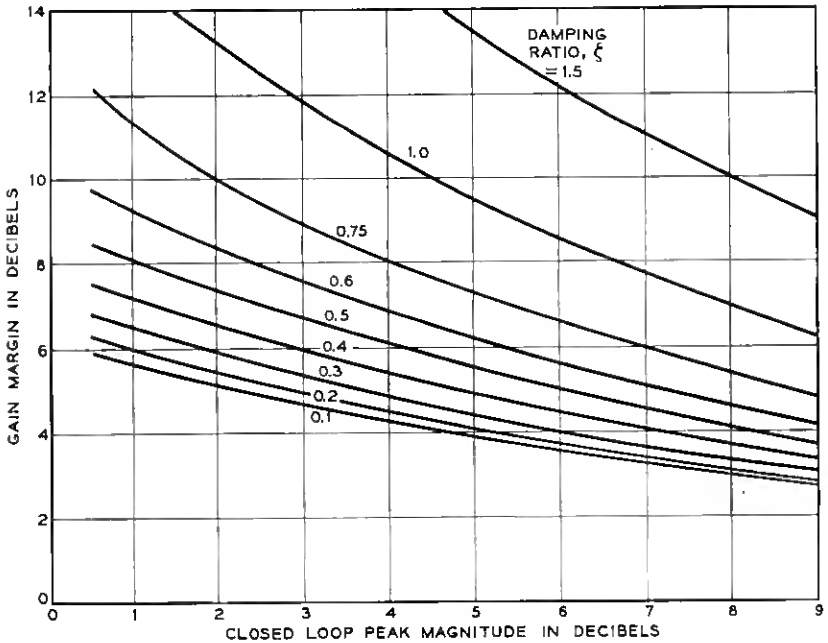

Fig. 9 — Gain margin vs. closed-loop peak magnitude as a function of damping ratio.

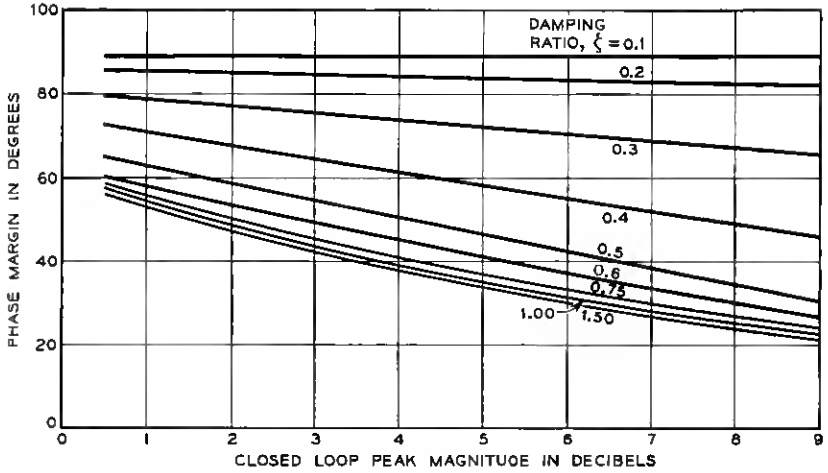

Fig. 10 — Phase margin vs. closed-loop peak magnitude as a function of damping ratio.

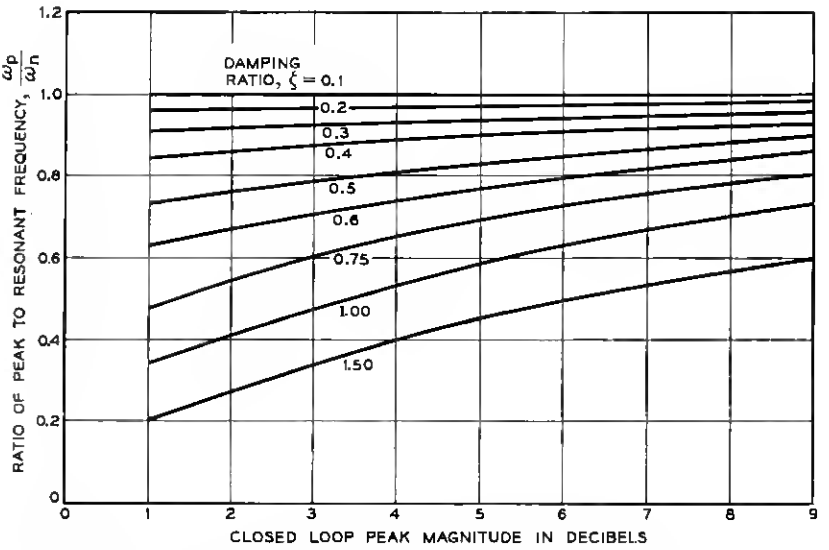

Fig. 11 — Closed-loop peak frequency vs. peak magnitude as a function of damping ratio.

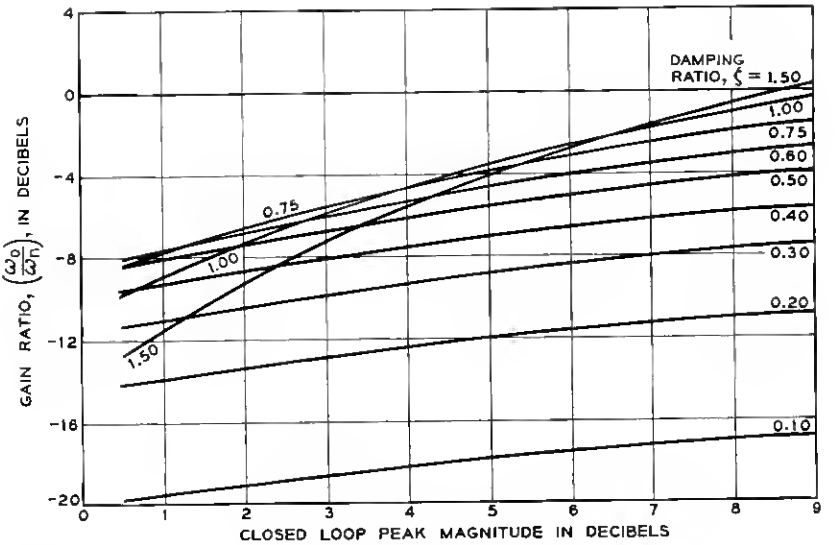

Fig. 12 — Gain ratio vs. closed-loop peak magnitude as a function of damping ratio.

for $\zeta = 1.00$, ω_0 must change 9 db for the same increase in peak magnitude. Since, in a practical system, fluctuations in the value of ω_0 are to be expected, operation of the lightly damped system would be more erratic than that of a system having adequate damping.

Equation (70), when solved for the transient response (θ_i a step function) yields solutions as given in Fig. 13. It is interesting to note that the transient response for a servomechanism having a damping ratio of $\zeta = 0.1$ and a closed-loop peak magnitude $M_p = 3$ db shows little overshoot. Examination of the frequency response shows that this is a result of a large attenuation in the frequency region below resonance. The superimposed oscillation is caused by the gain in the resonant frequency region.

The results of the transient solutions for $\zeta = 0.5$ are summarized in graphical form in Fig. 14, in which the delay time, T_d, rise time, T_r, peak time, T_p, and per cent overshoot are given as functions of the gain, ω_0/ω_n. (The definitions of the various time values are given in Fig. 15.) The response times decrease rapidly with increasing gain for the lower gain values and, as the gain increases, become relatively insensitive to gain variations. The per cent overshoot is a linear function of gain for values of gain above the limiting case in which there is no overshoot ($\omega_0/\omega_n = 0.316$).

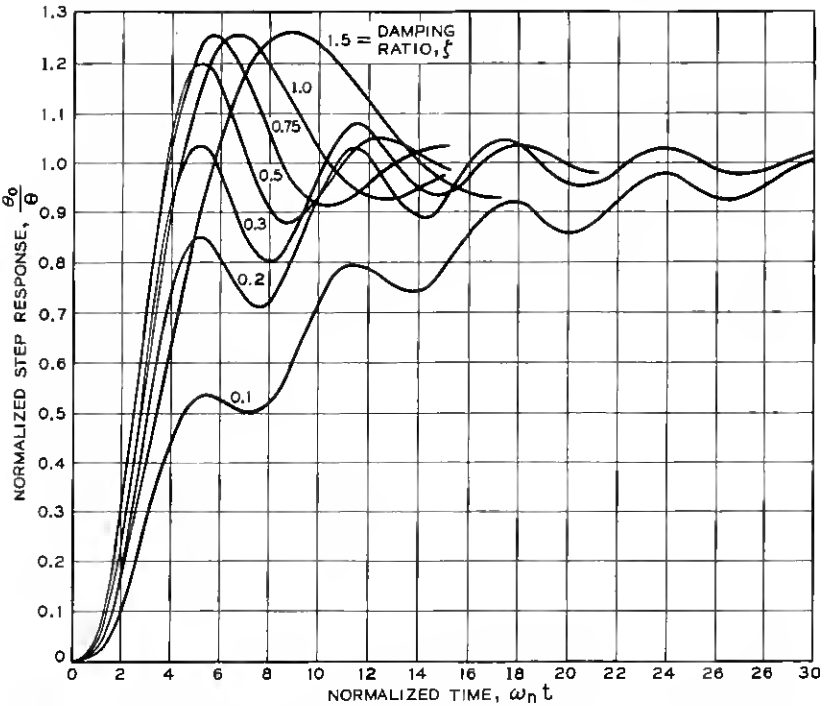

Fig. 13 — Variation of step response of linear system with damping ratio for constant closed-loop peak attenuation $M_p = 3$ db.

The relationships developed in this section can be used to estimate design parameters. For example, from Fig. 9, assume that a gain margin of 6 db is desired for a servomechanism having a damping ratio $\zeta = 0.5$. This fixes the peak magnitude M_p to be 4.15 db and, from Fig. 10, the phase margin is found to be 50 degrees. From Fig. 11, the peak frequency is $\omega_p = 0.8\ \omega_n$ and, from Fig. 12, the gain ratio ω_0/ω_n is -6 db; i.e., $\omega_0 = 0.5\ \omega_n$. Fig. 14 then predicts an overshoot of 24 per cent; a delay time, $T_d = 2.3/\omega_n$; a rise time, $T_r = 2.1/\omega_n$; and a peak time, $T_p = 5.0/\omega_n$.

VI. ANALOG SOLUTIONS OF THE NONLINEAR EQUATIONS

The equations representing the behavior of a valve-controlled servomechanism were derived in Sections II and III, and the approximate linear theory was discussed in Sections IV and V. In this section, representative analog computer solutions of the nonlinear equations (which

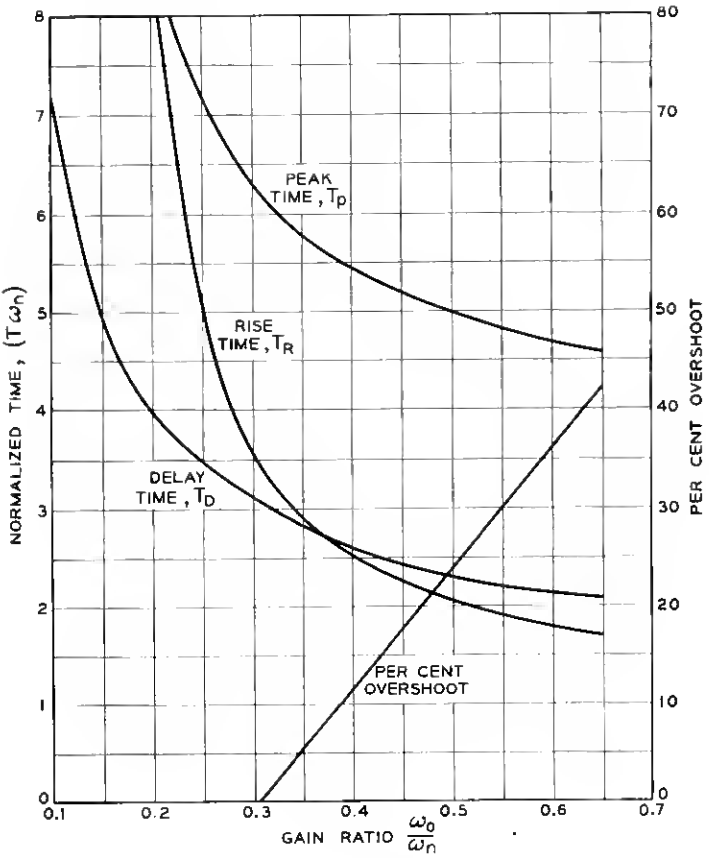

Fig. 14 — Transient response data for a damping ratio of 0.5.

are summarized in Table III) are given for particular values of the parameters, and the results are correlated with the linear solutions.

The valve-controlled servomechanism is assumed to have the numerical constants listed in Table IV. During the course of the discussion, the effects of changes in these parameters will be considered, but, unless otherwise stated, the values will be assumed to be as given in the table. In this manner, a reference system is obtained and the discussion of the effects of parameter variations is facilitated by comparison with the reference behavior.

The first eight constants listed in the Table IV are considered to be the independent variables while the remaining five are dependent. The compliance coefficient, K_c, is given by (16) as the ratio of V_T to β.

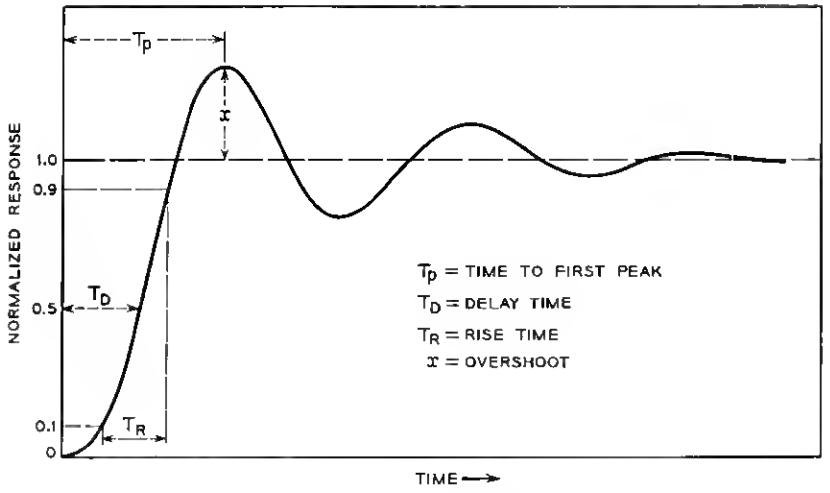

Fig. 15 — Definitions of transient symbols.

The effective leakage coefficient, L_a, is given by (50) as

$$L_a = L_m + \frac{K_b \epsilon_0}{\sqrt{2p_s}} \tag{71}$$

and the undamped natural frequency is given by (44) as

$$\omega_n = V_m \sqrt{\frac{2\beta}{V_T J}}. \tag{72}$$

TABLE III — EQUATIONS SOLVED BY ANALOG COMPUTATION

$$\begin{aligned}
Q_1 &= L_m(p_1 - p_2) + V_m\dot{\theta}_0 + K_c\dot{p}_1 \\
Q_2 &= -L_m(p_1 - p_2) - V_m\dot{\theta}_0 + K_c\dot{p}_2 \\
(p_1 - p_2)V_m &= J\ddot{\theta}_0 \\
\epsilon &= \theta_i - \theta_0 \\
p_1 &\geqq 0 \quad \text{and} \quad p_2 \geqq 0 \\
Q_1 &= Q_{O1} - Q_{E1} \\
Q_2 &= Q_{O2} - Q_{E2} \\
Q_{O1} &= \begin{cases} K_b \mid \epsilon + \epsilon_0 \mid \sqrt{\mid p_s - p_1 \mid}\ \operatorname{sgn}(p_s - p_1) & \epsilon > -\epsilon_0 \\ 0 & \epsilon < -\epsilon_0 \end{cases} \\
Q_{O2} &= \begin{cases} 0 & \epsilon > \epsilon_0 \\ K_b \mid \epsilon - \epsilon_0 \mid \sqrt{\mid p_s - p_2 \mid}\ \operatorname{sgn}(p_s - p_2) & \epsilon < \epsilon_0 \end{cases} \\
Q_{E1} &= \begin{cases} 0 & \epsilon > \epsilon_0 \\ K_b \mid \epsilon - \epsilon_0 \mid \sqrt{p_1} & \epsilon < \epsilon_0 \end{cases} \\
Q_{E2} &= \begin{cases} K_b \mid \epsilon + \epsilon_0 \mid \sqrt{p_2} & \epsilon > -\epsilon_0 \\ 0 & \epsilon < -\epsilon_0 \end{cases}
\end{aligned}$$

TABLE IV — REFERENCE VALUES OF PARAMETERS

Definition	Symbol	Value	Units
total inertia	J	2.73×10^{-3}	lb-in-sec^2
motor displacement	V_m	0.0151	in^3
trapped volume	V_T	0.125	in^3
bulk modulus	β	2.22×10^5	lb/in^2
motor leakage coefficient	L_m	0.039×10^{-3}	in^5/lb-sec
supply pressure	p_s	1000	lb/in^2
gain constant	K_b	0.0912	in^4/lb$^{1/2}$-sec-rad
open-center constant	ϵ_0	0.0561	radians
		3.21	degrees
compliance coefficient	K_c	0.0563×10^{-5}	in^5/lb
effective leakage coefficient	L_a	0.1533×10^{-3}	in^5/lb-sec
resonant frequency	ω_n	544.7	rad/sec
		86.6	cps
damping ratio	ζ_a	0.5	
gain ratio	$\frac{\omega_a}{\omega_n}$	0.496	

The dimensionless damping ratio ζ_a [from (51)] is

$$\zeta_a = \frac{L_a}{V_m}\sqrt{\frac{J\beta}{2V_T}}, \tag{73}$$

and the velocity gain constant is obtained from (46):

$$\omega_a = \frac{2K_b}{V_m}\sqrt{\frac{p_s}{2}}. \tag{74}$$

Fig. 16 shows the theoretical frequency response of the reference servomechanism as a function of the input amplitude. The linear prediction (based on small amplitudes and pressure differentials) is included for comparison. The amplitude sensitivity in the small signal region, as represented for example by a curve of 1° amplitude, is the result of the nonlinear flow characteristics of the valve. The operation is within the region in which $|\epsilon| < \epsilon_0$ (A region) and pressure saturation has not occurred.†

The response for an input of 2° shows more deviation from the linear response, primarily because of pressure saturation; operation is still within the A region. For greater input amplitudes, the response falls off

† A −12 db per octave slope that passes through zero db at the frequency

$$[f_{\text{lim}}]_{0\text{ db}} = \frac{1}{2\pi}\sqrt{\frac{p_s V_m}{J\theta_i}}$$

divides the graph into regions that represent the saturating and nonsaturating conditions.

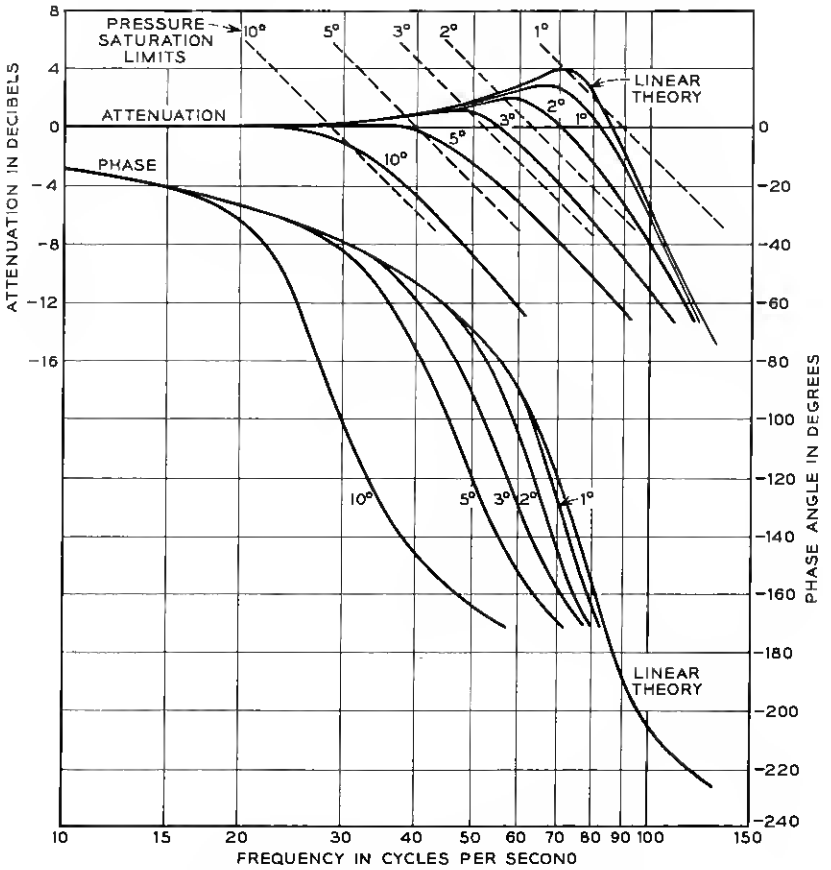

Fig. 16 — Theoretical frequency response of a hydraulic servomechanism as a function of input amplitude.

rapidly and operation is primarily in the B region; pressure saturation effects become more pronounced.

The closed-loop transient response of the reference system as a function of step magnitude is given in Fig. 17, together with the linear solution. For small amplitudes (less than 3°), the linear and nonlinear solutions are essentially identical; as the amplitude is increased, the discrepancy becomes large. The per cent overshoot decreases with amplitude.

It is evident that the transient response of the servomechanism is not as sensitive to amplitude as is the frequency response; for example, comparison of the 3° curves in Figs. 16 and 17 shows that the transient

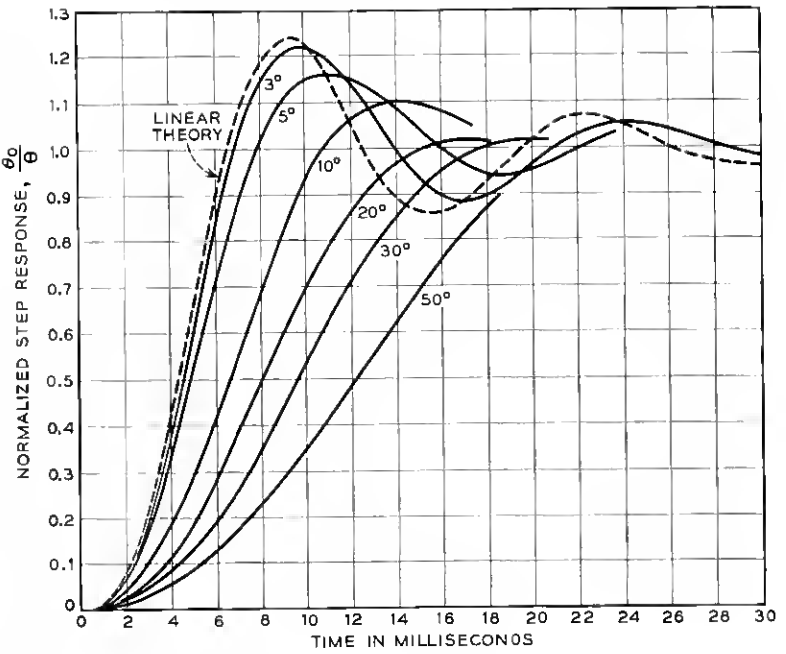

Fig. 17 — Theoretical transient response of hydraulic servomechanism as a function of amplitude.

is much closer to the linear transient solution than the frequency response is to the linear frequency response. This difference is attributable mainly to pressure saturation. Fig. 18 shows the transient response of the system for the 3° step, together with the pressures p_1 and p_2. Since the supply pressure is 1000 psi and the valve is symmetrical, both pressures are initially 500 psi in the quiescent condition. For the case shown, the applied step was in the positive direction, so that θ_0 was also positive; consequently, p_1 has an initial positive slope while p_2 has a negative slope. From 0 to 2 milliseconds, the oil is compressed and very little shaft rotation occurs; maximum acceleration $(p_1 - p_2)$ occurs at 2 milliseconds, at which time the shaft has acquired an appreciable velocity. From 2 to 5 milliseconds, the acceleration decreases from maximum to zero, while the velocity continues to increase to its maximum value. From 5 to 6.8 milliseconds, the acceleration becomes negative, since p_2 is now greater than p_1. The velocity is still positive for this period, and the error signal ϵ decreases from a positive value to zero. The increase in p_2 is due to the compression of the oil in line 2 by the moving inertia, as the orifice area opening to the sump is gradu-

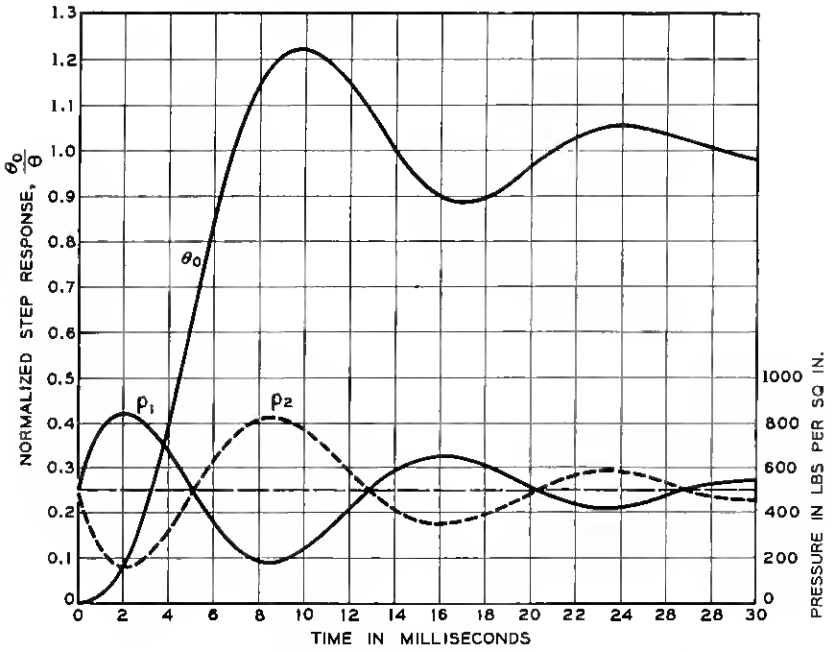

Fig. 18 — Output and pressure variation with time for a 3° step.

ally reduced and the pump pressure is applied to this side of the motor. For the period from 6.8 to 9.5 milliseconds, the error ϵ is negative and the velocity decreases to zero at the peak of the curve.

The nature of the response after 9.5 milliseconds is very similar to that previously described, since the output starts from rest with an initial error. The major difference, aside from the fact that the error is now negative, is that the pressures have appreciable values at 9.5 milliseconds, while at 0 milliseconds the pressures started from the quiescent state.

It should be noticed that the pressures p_1 and p_2 did not limit for the 3° step and that, although the pressure differentials were appreciable, the linear theory still provided a good approximation to the output motion, as indicated in Fig. 17. The value of ϵ_0 as given in Table IV is 3.2°, so that operation was entirely within the A region.

Fig. 19 shows the transient response and pressures for the 20° step. In this case, the pressures just limit at the start, and the pressure differentials are large. In Fig. 20, for the 30° step, the initial pressure saturation is more pronounced and, in addition, p_1 reaches zero and p_2 obtains

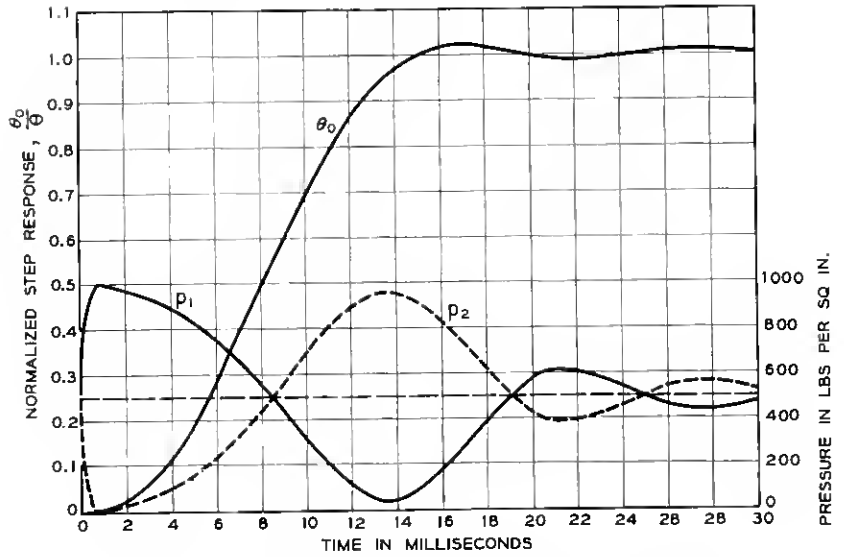

Fig. 19 — Output and pressure variation with time for a 20° step.

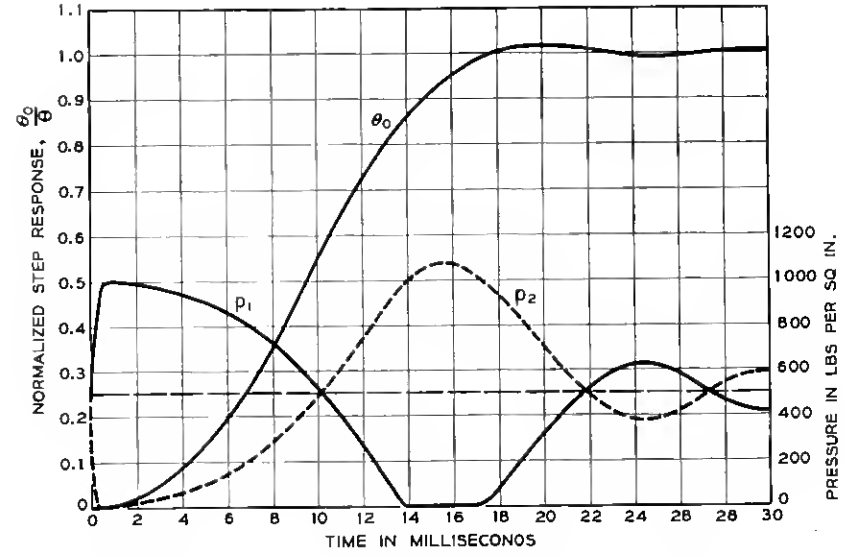

Fig. 20 — Output and pressure variation with time for a 30° step.

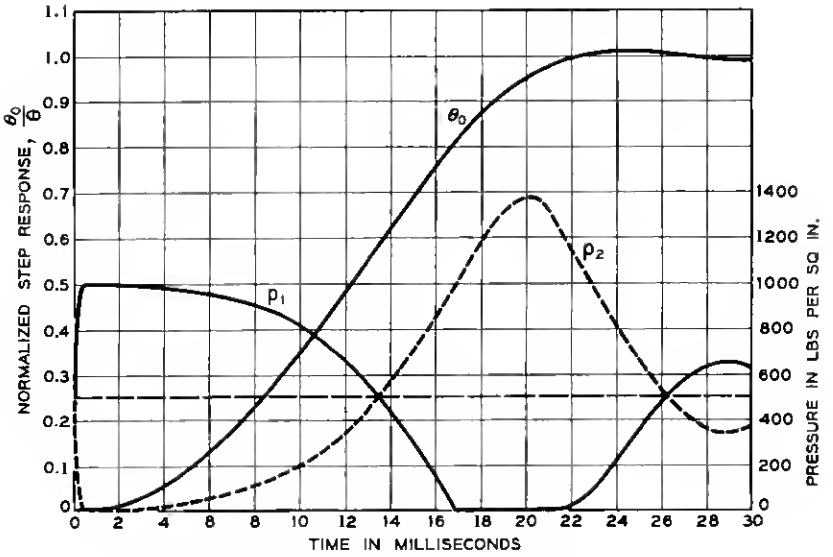

Fig. 21 — Output and pressure variation with time for a 50° step.

a value above that of the supply pressure (p_s = 1000 psi). Examination of the curves shows that the maximum value of p_2 of 1080 psi occurs for ϵ positive, the velocity positive and the acceleration negative. This indicates that the inertia of the motor and load combination is forcing oil to flow out of the exhaust orifice and that, as a result, the pressure p_2 achieves a very high value. At the same time, oil is forced through the orifice connecting the pressure supply to line 1, but the velocity is so great that the rate of flow is not sufficient to maintain a pressure in this line. Thus, during the period from 14 to 17 milliseconds cavitation conditions exist on this side of the motor.

In Fig. 21, for the 50° step, the situation is similar to that of Fig. 20, except that the saturation and cavitation periods are of longer duration. Here, the peak pressure is very nearly 1400 psi.

From the preceding discussion, the desirability of including relief valves in each line is apparent. Dangerously high pressures can be generated, especially if a supply pressure of 3000 psi is used. The inclusion of relief valves in effect limits the line pressure, so that the oil cannot be "trapped" by the inertia. This, however, has the disadvantage of increasing the overshoot for large amplitudes and does not decrease the rise or delay times. In addition, the cavitation period is prolonged.

The effect of the variation in gain, K_b, is shown in Figs. 22 and 23.

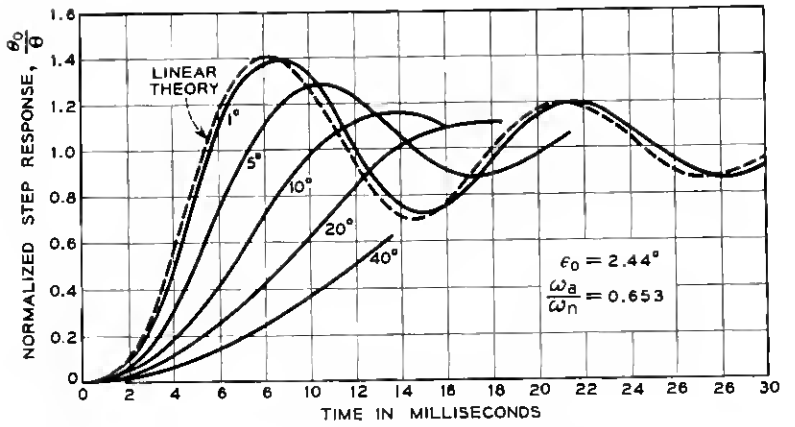

Fig. 22 — Theoretical transient response as a function of amplitude for $K_b = 0.12$.

In Fig. 22, K_b has a value of 0.12, so that the parameters listed on the figure change from those of the reference case; all other parameters remain constant as given in Table IV. Since the open-center constant ϵ_0 is now only 2.44°, it is to be expected that the system exhibit more amplitude sensitivity. Comparison with Fig. 17 shows that this is the case; in the small-signal region, the curves for the higher-gain system differ somewhat more from the linear solution than do those in Fig. 17.

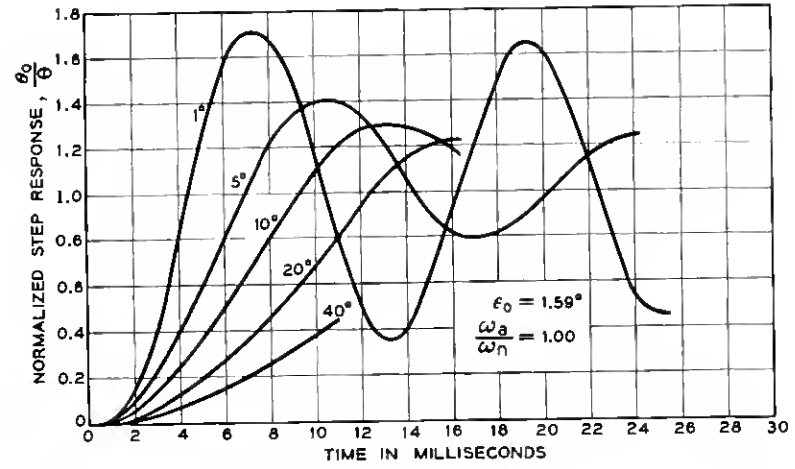

Fig. 23 — Theoretical transient response as a function of amplitude for $K_b = 0.184$.

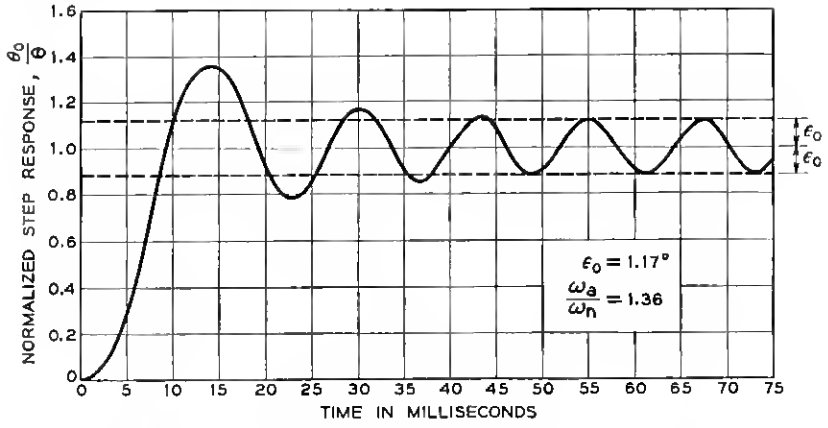

Fig. 24 — Transient response for a 10° step with $K_b = 0.25$.

As the amplitude increases, this effect is lost, and the major difference is found in the per cent overshoot.

In Fig. 23, the gain constant, K_b, is 0.184. For this value the dimensionless gain ratio is unity and the linear theory predicts zero gain margin. There is a distinct difference in the nature of the response as the amplitude increases. For the 1° step, the operation is entirely within the A region ($\epsilon_0 = 1.59°$) and the oscillations are almost continuous. As the amplitude increases, the per cent overshoot decreases, since pressure saturation occurs.

This effect on the stability is more pronounced at the higher gain values. In Fig. 24, a 10° step is shown for the case in which $K_b = 0.25$ and the gain ratio is 1.36. From the linear theory, this system should be unstable. Examination of the response shows that, in the A region in which ϵ is less than $\epsilon_0 = 1.17°$, the system is unstable, but that it is stable in the B region in which ϵ is greater than ϵ_0. The response, therefore, oscillates indefinitely, but only with the amplitude of ϵ_0. It is evident, therefore, that, if frictional forces are sufficient to overcome the small oscillations of $\pm\epsilon_0$ amplitude, or if these oscillations are not detrimental to the performance in the particular application, the allowable gain is much greater than that predicted by the linear theory. For a given valve, $K_b\epsilon_0$ is a constant, so that, as the gain K_b is increased, the magnitude ϵ_0 of the sustained oscillations decrease. The incremental damping and gain constants for the B region are given by (57) and (59); these equations show that the operation in the B region is inherently more stable than that in the A region, since the incremental damping

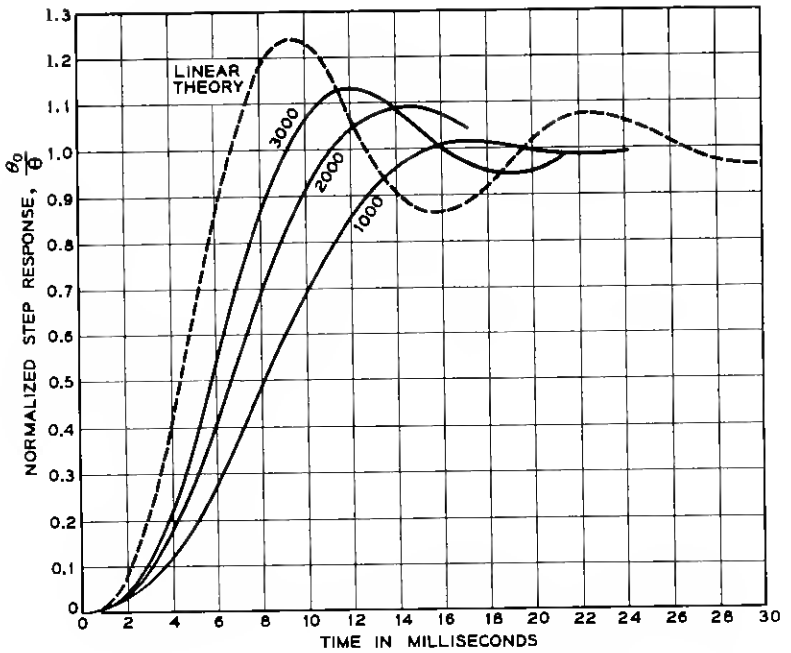

Fig. 25 — Transient response as a function of supply pressure for a 20° step.

is greater than in the A region and the incremental gain is less than the corresponding A region gain. Thus, in the absence of friction or viscous damping, the sustained oscillations are most pronounced in the A region.

The effect of the supply pressure on the transient response is shown in Fig. 25 for a 20° step. The linear theory provides the best approximation for the case in which the supply pressure is greatest. This is the result of two factors: (a) the system with the higher pressure is less susceptible to pressure saturation and (b) the value of ϵ_0 increases with increasing supply pressure, so that operation is more completely in the A region. The solutions show that, whereas the system having a supply pressure of 1000 psi encounters saturation for a 20° step, the 3000-psi servo is not pressure-limited until subjected to a 60° step. The advantage of operating at higher pressures is thus primarily a question of pressure saturation.

In all the previous solutions, the effective leakage coefficient, L_a, has been maintained constant at 0.1533×10^{-3} inches^5 per pound-second, so that the damping ratio, ζ_a, was 0.5. From (71), it is seen that the effective leakage coefficient is the sum of the motor leakage

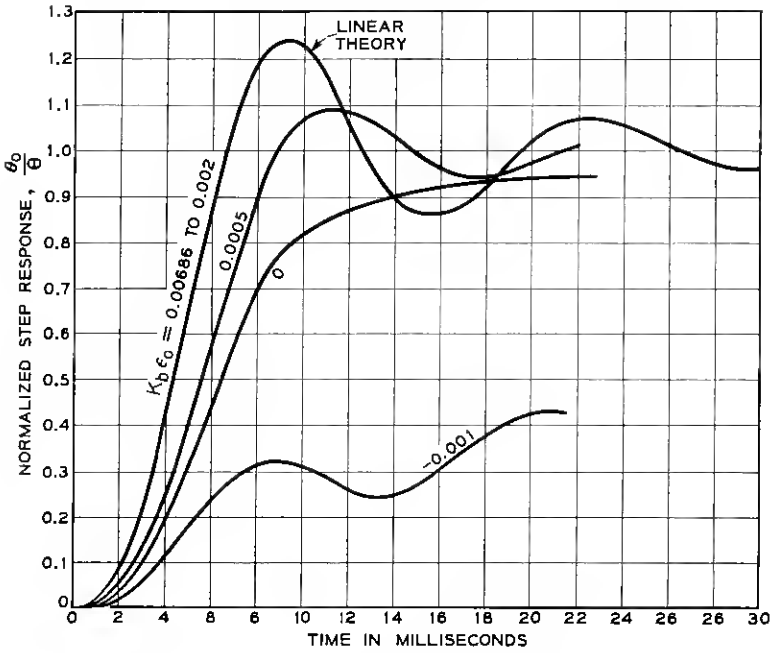

Fig. 26 — Theoretical transient response as a function of $K_b\epsilon_0$ for a 1° step.

coefficient and a term proportional to $K_b\epsilon_0$. It is interesting to observe the response of the system as affected by the nature of the damping. This is given in Fig. 26 for a 1° step. The three upper curves have a damping ratio of $\zeta_a = 0.5$; the difference in the curves results from the method used in obtaining the damping. For cases in which the open-center valve provides appreciable damping, the response does not differ from the linear prediction. This is the result of operation in the A region, where ϵ is less than ϵ_0. As the valve damping decreases and the motor leakage is increased, the response is slower and falls below the linear curve; this occurs for the case in which $K_b\epsilon_0$ is 0.0005. Operation is partly in the B region, since ϵ_0 is equal to 0.31°.

When the damping is contributed entirely by the motor leakage, $K_b\epsilon_0 = 0$ and the valve is of the critical-center type. In this case, Fig. 26 shows that the response does not overshoot and that an increase in gain would be desirable. Computer results show that, for $K_b = 0.20$, the critical-center valve gives a transient response having about 25 per cent overshoot and adequate stability. However, it should be emphasized that the damping ratio for this case was 0.5 and that the damping

was obtained by altering the motor leakage. Any attempt to reduce the valve-quiescent flow without compensating the system in some manner to provide additional damping results in an underdamped servomechanism.

The final curve, for which $K_b\epsilon_0 = -0.001$ in Fig. 26, represents the response to be expected with a closed-center valve. This valve has a dead zone of 0.63° about which the output will wander, and is shown in a particularly poor case, since the step is only 1° and the gain is small. The only damping in this system is contributed by motor leakage, so that the system is underdamped.

VII. CONCLUSIONS

This study shows that the linear approximation to the nonlinear representation of valve-controlled hydraulic servomechanisms can be applied only with the sacrifice of considerable accuracy. However, since the linear theory is readily applied, it can be used in obtaining estimates for preliminary designs if the deviations from the nonlinear solutions are understood.

REFERENCES

1. Schaefer, J. W., An Electrically Operated Hydraulic Control Valve, B.S.T.J., **36**, May 1957, p. 711.
2. Blackburn, J. F. and Lee, S. Y., Contributions to Hydraulic Control — 1. Steady-State Axial Forces on Control-Valve Pistons, Trans. A.S.M.E., **74**, August 1952, p. 1005.
3. Blackburn, J. F., Contributions to Hydraulic Control — 3. Pressure-Flow Relationships for 4-Way Valves, Trans. A.S.M.E., **75**, August 1953, p. 1163.
4. Shearer, J. L., Dynamic Characteristics of Valve-Controlled Hydraulic Servomotors, Trans. A.S.M.E., **76**, August 1954, p. 895.